Numerical Modeling of Litz Wires Based on Discrete Transpositions of Strands and 2-D Finite Element Analysis

Silvano Cruciani, Tommaso Campi, Francesca Maradei, and Mauro Feliziani

***Abstract*—A new numerical method is proposed to model the electric behavior of a single bundle litz wire with a large number of strands. The method is first based on a two-dimensional (2-D) finite element analysis (FEA) to evaluate the series impedance matrix of a multistrand cable with parallel strands. Then, a mathematical algorithm for a discrete transposition of all strands is applied to simulate the bunching and twisting of the strands. The new procedure is very efficient and accurate, as demonstrated by the excellent agreement of the numerical results with those obtained by experiments or with 3-D FEA. The error in terms of ac-to-dc resistance ratio is less than 10% in the tested configurations. Furthermore, the computational cost of the proposed method is very low and comparable with a simple 2-D FEA.**

***Index Terms*—Finite element analysis (FEA), inductive coils, inductive power transfer (IPT), litz wire, skin and proximity effects, wireless power transfer (WPT).**

I. Introduction

LITZ wires are widely used in many application fields of power electronics as they strongly mitigate the skin and proximity effects, thus reducing the ac losses. Currently there is an increasing interest on litz wires due to their wide use in the emerging technology known as wireless power transfer (WPT) and based on inductive coupling [1], [2]. In this technology, the conductors used for the coils are often made by litz wires and the coils are generally in air. Thus, the magnetic field in WPT applications is lower than that of traditional inductors with magnetic core, but the frequency is higher than powerline frequency (e.g., 50/60 Hz). Typical operating frequencies in WPT applications using litz wire coils range from tens of kilohertz to a few megahertz.

The goal of this study is the development of an accurate numerical model of litz wires for WPT applications. Predicting the ac resistance with good accuracy is therefore very important since the resistance appears in the Q factor expression of inductors. A litz wire is a multistrand conductor where each strand is a thin, insulated conductor (generally made of copper with diameter $d < 1$ mm and enameled). The number n of conductive strands can be very high, i.e., $n > 1000$. The strands are often grouped in bundles and twisted to reduce the skin and proximity effects.

The challenge in litz wire design consists in adopting complex bunching architectures to obtain an approximately identical path for all strands, which therefore occupy all possible positions in the litz wire sections. In an ideal pattern model, the impedance of all the strands is the same and the current flowing through each of them is also the same. Therefore, the distribution of the current in any cross section of litz is quite uniform and insensitive to skin and proximity effects. A drawback of this bunching strategy is the increase in the length of the strands due to the twist resulting in a small increase in power losses. Despite the real manufacture of litz wires cannot completely satisfy the ideal pattern of the strands, in practical applications, the performance expressed as the ratio F_r between the ac resistance and dc resistance is quite good ($1 \leq F_r \leq 2$ at the operational frequency).

Litz wire modeling is not easy. In the past, complex analytical formulations have been provided based on some simplifying hypotheses [3], [4], [5] [6], [7], [8], [9], [10], [11], [12], [13]. In recent times, thanks to the ever-increasing performance of software and computers, some studies based on numerical models have been presented [14], [15], [16], [17], [18], [19], [20], [21], [22], [23], [24], [25], [26], [27], [28]. The numerical methods are very complex and are mainly based on the finite element analysis (FEA) solving eddy currents equations in the frequency domain. The configuration of a litz wire is typically three-dimensional (3-D) due to the twisting of strands and bundles, thus the generation of the finite element mesh and the computation are very heavy and often impracticable even when the number of strands is not so high. In fact, the size of the finite elements in the conductors must be much less than the penetration depth, and therefore, the mesh must be very fine to accurately take into account the skin and proximity effects. To overcome this

Manuscript received 29 May 2022; revised 19 September 2022 and 19 December 2022; accepted 20 January 2023. Date of publication 3 February 2023; date of current version 10 March 2023. Recommended for publication by Associate Editor Z. Zhang. *(Corresponding author: Tommaso Campi.)*

Silvano Cruciani is with the Department of Industrial Engineering, University of Rome "Tor Vergata", 00133 Roma, Italy (e-mail: silvano.cruciani@uniroma2.it).

Tommaso Campi and Mauro Feliziani are with the Department of Industrial and Information Engineering and Economics, University of L'Aquila, 67040 L'Aquila, Italy (e-mail: tommaso.campi8888@gmail.com; mauro.feliziani@univaq.it).

Francesca Maradei is with the Department of Astronautics, Electrical and Energetics Engineering, University of Rome "La Sapienza", 00184 Rome, Italy (e-mail: francesca.maradei@uniroma1.it).

Color versions of one or more figures in this article are available at https://doi.org/10.1109/TPEL.2023.3240338.

Digital Object Identifier 10.1109/TPEL.2023.3240338

inconvenience, several numerical approaches have been proposed using circuit equations or homogenization techniques [28], [29], [30], [31].

Here, an innovative and simple simulation method is proposed to model a multistrand litz wire, which is seen as a nonuniform multiconductor transmission line (MTL). In the past, the transmission line theory was applied to model nonuniform lines adopting a segmentation approach. The segmentation approach was originally proposed in [32] and [33] to predict crosstalk in twisted-wire pairs, which were modeled as a cascade of loops consisting of uniform two-wire sections with abrupt interchanges of wire positions at the ends of each loop. A further development of this approach was proposed in [34] to evaluate the voltage and current wave propagation in a nonuniform MTL with helical conductors. The MTL was discretized into small sections, each considered as a uniform line with parallel conductors. The circuit parameters of each section were obtained by means of a two-dimensional (2-D) FEA [35], [36], [37], [38]. The computational cost increases with the number of sections used in the discretization. The uniform MTL sections were then cascaded to obtain an equivalent circuit model suitable for analysis by CAD circuit simulators. This approach, based on the segmentation of a nonuniform MTLs into small sections of cascaded uniform line, can be also applied to a litz wire, which is an MTL with shorted ends. However, in the case of a large number of strands, the number of sections to be used in the segmentation becomes very high, and therefore, this approach would be extremely demanding in terms of computational resources since the series impedance matrix must be calculated for any segment and the strands must be connected physically at any segment interface. To overcome this drawback, a new numerical procedure is proposed, which is very convenient from a computational point of view as it is based on a single 2-D FEA to obtain the series impedance matrix of a reference litz wire section [35]. Passing from one section to the next, it is assumed that each strand moves discretely to a new position among those included in the reference section. The model of the nonuniform litz wire is then obtained by mathematically applying a large number of discrete transpositions to all strands to simulate an ideal twisting (i.e., all strands are assumed to have the same impedance and current as demonstrated in several studies [16], [28]). By this approach, it is not necessary to consider the real strand connections between different cascaded MTL segments and the numerical cost of the procedure is relatively low and comparable to a 2-D FEA.

It should be noted that a procedure based on the segmentation approach was also proposed in [28] for concentric twisted litz wires with some simplifying assumptions. Concentric litz wires are layered in concentric circles and strands are moving during the twisting remaining in the same layer. The impedance of each strand in the same layer is almost the same, but different in different layers. The approach proposed here is instead valid for any litz wire and it is based on the assumption that the strands have all the same impedance. This is reasonably achieved in the proposed algorithm by allowing each strand to occupy any possible positions inside the cable. Although the transposition algorithm proposed in this work is only mathematical, without any close relation with the real physical twisting of the strands, it provides very accurate results as clearly demonstrated in Section III. Another great advantage of the proposed method is the possibility to easily varying some geometrical parameters of the litz wire configuration. This aspect is very important in the design and optimization of a coil for WPT systems.

In the following, the mathematical method of the proposed numerical procedure is first presented and then validated by comparison with experimental and 3-D numerical results. The validation performed adopting different configurations of single bundle litz wires testifies an excellent accuracy in terms of ac resistance.

II. Mathematical Model

A. Litz Wire Configuration

Litz wires have been introduced to reduce the ac power losses, by mitigating both skin and proximity effects. AC power loss in a strand increases with increasing frequency as the current tends to distribute in the external part of the conductor (strand level skin effect). This skin effect is significant when the strand diameter d is greater than the penetration depth $\delta = 1/\sqrt{\pi f \mu \sigma}$, being f the frequency, μ the permeability, and σ the conductivity of the strands. At the operational frequency, the strand diameter is typically designed as $d < \delta / 3$ [39], [40]. Following this rule, d can be very small and the current that can flow in it is also very small. Therefore, the number n of the strands in a litz wire can become very large to carry the amount of current required for the application under consideration. At low frequency, the strand level skin effect is negligible as the current distribution is fairly constant in the strand section as in dc. When considering a bundle of parallel strands, the current tends to distribute itself more in the external strands of the bundle (bundle level skin effect).

The proximity effect is due to the action of the magnetic field that can modify the distribution of the current inside the strands increasing the ac power loss due to circulating currents. The magnetic field can be produced by the current flowing in other nearby strands (strand level proximity effect), bundles (bundle level proximity effect), or other sources (external field proximity effect). Strand level and bundle level skin and proximity effects depend on the electrogeometric configuration of the litz wire, as well described in the technical literature [4], [5], [6], [7].

Litz wires with low numbers of strands typically consist of a single bundle. Litz wires with higher numbers of strands are often made of several bundles twisted and bunched together. The length of lay (pitch p) describes the distance that a single wire needs for a full rotation (360°) around the circumference of the strand, as shown in Fig. 1 [39].

B. Litz Wire Modeled by Parallel Strands

A litz wire composed by n independent strands is initially assumed to be a uniform MTL, i.e., all strands are assumed to be straight and parallel. The voltage and current vectors of the n insulated strands are described by the low frequency equation

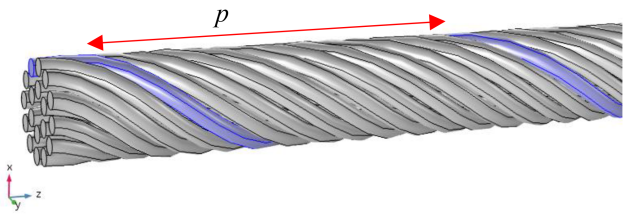

Fig. 1. Pitch p (or length of lay).

valid for an electrically short line as

$$\mathbf{V}_0 - \mathbf{V}_l = \mathbf{z}\ell\mathbf{I} \tag{1}$$

where $\ell << \lambda$ is the length of the considered line, being λ the wavelength, $\mathbf{V}_0$ and $\mathbf{V}_l$ are the voltage vectors of n rows at $x = 0$ and $x = \ell$, respectively, $\mathbf{I}$ is the current vector of n rows, and $\mathbf{z}$ is the $n \times n$ per-unit-length (p.u.l.) impedance matrix. The impedance matrix $\mathbf{Z} = \mathbf{z}\ \ell$ can be evaluated by a numerical approach based on the solution of eddy currents equations by the FEA [35]. The 2-D FEA is carried out neglecting the capacitances and therefore, the proposed approach is not valid for modeling the high frequency behavior of a litz wire.

To predict $\mathbf{Z}$, n simulations are performed imposing n different excitations. From a mathematical point of view, the applied voltages of the generic kth simulation can be grouped in the voltage vector $\mathbf{V}^{(k)} = \mathbf{V}_0{}^{(k)} - \mathbf{V}_l{}^{(k)}$. Assuming a unit voltage excitation $V_a = 1$ V, the ith coefficient of $\mathbf{V}^{(k)}$ is given by $V_i^{(k)} = V_a$ for $i = k$ and $V_i^{(k)} = 0$ for $i \neq k$. Therefore, it yields: $\mathbf{V}^{(1)} = [V_a\ 0\ 0\ \ldots\ 0]^{\mathrm{T}}$, $\mathbf{V}^{(2)} = [0\ V_a\ 0\ \ldots\ 0]^{\mathrm{T}}$, …, $\mathbf{V}^{(n)} = [0\ 0\ 0\ \ldots\ V_a]^{\mathrm{T}}$.

The currents flowing in the n strands obtained in the kth simulation are assembled into the corresponding vector $\mathbf{I}^{(k)} = \left[I_1^{(k)}\ \ I_2^{(k)}\ \ \cdots\ \ I_n^{(k)}\right]^T$ where the coefficient $I_i{}^{(k)}$ is the generic ith strand current at kth simulation. At the end of the n simulations, the following system is obtained where all matrices are of order $n \times n$:

$$\left[\ \mathbf{V}^{(1)}\ \ \mathbf{V}^{(2)}\ \ \ldots\ \ \mathbf{V}^{(n)}\ \right] = \mathbf{Z}\left[\ \mathbf{I}^{(1)}\ \ \mathbf{I}^{(2)}\ \ \ldots\ \ \mathbf{I}^{(n)}\ \right]. \tag{2}$$

As an equal voltage excitation was assumed (e.g., $V_a = 1$ V), the voltage matrix in (2) is $V_a\ \mathbf{1}$ being $\mathbf{1}$ the identity matrix and the series impedance matrix $\mathbf{Z}$ is then obtained as

$$\mathbf{Z} = V_a\left[\ \mathbf{I}^{(1)}\ \ \mathbf{I}^{(2)}\ \ \cdots\ \ \mathbf{I}^{(n)}\ \right]^{-1}. \tag{3}$$

Once the impedance $\mathbf{Z}$ is known, it is possible to evaluate the current distribution in all strands for any voltage excitation by the following equation derived from (1):

$$\mathbf{I} = \mathbf{Y}\left(\mathbf{V}_0 - \mathbf{V}_l\right) \tag{4}$$

where $\mathbf{Y} = \mathbf{Z}^{-1}$. In litz wire applications, the strands are connected in parallel at $x = 0$ and $x = \ell$, so all coefficients of voltage vectors $\mathbf{V}_0$ and $\mathbf{V}_l$ are equal to the applied scalar voltages V_0 and V_l, respectively, as

$$\mathbf{V}_0 = \left[\ V_0\ \ V_0\ \ \cdots\ \ V_0\ \right]^T = V_0\left[\ 1\ \ 1\ \ \cdots\ \ 1\ \right]^T \tag{5}$$

$$\mathbf{V}_l = \left[\ V_l\ \ V_l\ \ \cdots\ \ V_l\ \right]^T = V_l\left[\ 1\ \ 1\ \ \cdots\ \ 1\ \right]^T. \tag{6}$$

The current vector $\mathbf{I}$ is obtained from (4) and its ith coefficient (i.e., current flowing in the ith strand) is given by

$$I_i = V_a \sum_{k=1}^{n} Y_{ik} \tag{7}$$

when assuming the applied voltage $V_a = V_0 - V_l$, and being $Y_{i,k}$ the coefficient on row i and column k of the matrix $\mathbf{Y}$.

The litz wire current I_W is obtained as the sum of all strand currents as

$$I_W = \sum_{k=1}^{n} I_k. \tag{8}$$

The litz wire impedance Z_W can be calculated by Ohm's law as

$$Z_W = \frac{V_a}{I_W}. \tag{9}$$

The ac resistance R_{ac} of a litz wire is derived as

$$R_{\mathrm{ac}} = \mathrm{real}\left(Z_W\right). \tag{10}$$

The dc resistance R_{dc} can be simply calculated for a multistrand uniform line by the following formula:

$$R_{\mathrm{dc}} = \frac{\ell}{n\sigma\pi(d/2)^2} \tag{11}$$

where σ is the electrical conductivity of the strands, n is the number of strands, and d is the diameter of the conductive strand without considering the insulation layer of the enamel.

An important parameter of a litz wire is the ac-to-dc resistance ratio F_R defined as

$$F_R = \frac{R_{\mathrm{ac}}}{R_{\mathrm{dc}}}. \tag{12}$$

C. Litz Wire Modeling With Strand Transposition

The previous equations are valid for a uniform line with parallel strands, whereas the strands in a litz wire are bunched and twisted to minimize the skin and proximity effects. Although a realistic modeling should use a 3-D field approach to evaluate Z_W impedance, a 3-D numerical solution is a difficult and time-consuming job and requires a high computational cost. To overcome these drawbacks, a simple calculation method is proposed here based on the hypothesis of an ideal twist for all the strands, which are assumed to have the same path inside the litz wire. The problem now is how to impose this ideal twisting to a litz wire. In the proposed approach, the configuration of a single bundle litz wire is modeled as a series cascade of identical uniform wire sections with a transposition of the strands passing from one section to the next. Each wire will thus assume all possible positions within the cable, passing from one section to another within a pitch.

Given a reference cross section of a multistrand cable, the positions of the n strands are numbered to indicate the discrete positions that a strand can assume. A change in the relative position of the n strands along the line axis is accomplished by a discrete transposition of all strands, which is mathematically performed, without considering the real physical connection.

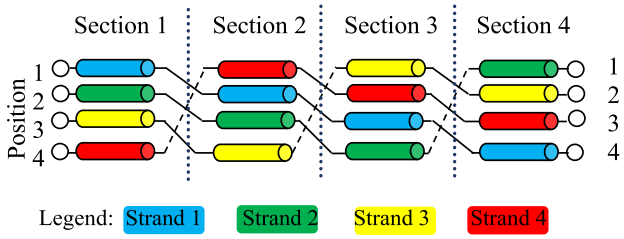

Fig. 2. Transposition of the strand positions in a segmented litz wire with $n = 4$ strands and $m = 4$ wire sections.

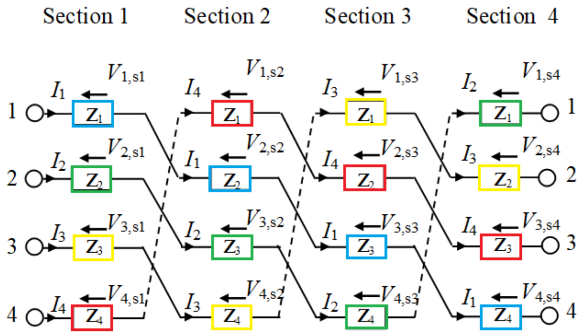

Fig. 3. Equivalent circuit model with transposition for $n = 4$ strands and $m = 4$ wire sections assuming that the impedance matrix is diagonal (only to better explain the proposed algorithm, whereas the real impedance matrix is full).

First, the litz wire of length ℓ is arbitrarily discretized into m line sections of equal length ℓ/m. A section is modeled as a multistrand line composed by n straight and parallel conductors. The impedance matrix for a section is given by $\mathbf{Z_s} = \mathbf{z}\,\ell/m$, being $\mathbf{z}$ the p.u.l. impedance matrix. During the transposition, each strand changes its position within the litz wire following a simple iterative algorithm. Assuming that all line section terminals are coded with numbers, the output terminal of the considered section is connected to the input terminal of the next section whose code has a number greater than one with respect to that of the output terminal considered. To better illustrate the transposition procedure, Fig. 2 shows a circuit diagram of the transposition scheme when assuming only four sections ($m = 4$) and four strands ($n = 4$) for simplicity. The strands of the litz wire are marked with a number and the positions that the strands occupy within the bundle cross section are also marked with a number. Each strand is color coded so that the variations of the strand position inside the litz wire can be easily observed.

The equivalent circuit is shown in Fig. 3 where, for simplicity, only the series impedance of each strand is shown. It should be noted that in a real litz wire, the matrix $\mathbf{Z_s}$ is a full matrix where off diagonal mutual terms Z_{ij} are nonzero. The diagonal series impedance matrix $\mathbf{Z}_s$ for each MTL section is given by

$$\mathbf{Z}_s = \begin{bmatrix} Z_1 & 0 & 0 & 0 \\ 0 & Z_2 & 0 & 0 \\ 0 & 0 & Z_3 & 0 \\ 0 & 0 & 0 & Z_4 \end{bmatrix}. \tag{13}$$

The vector of the strand currents flowing into the kth line section is indicated as $\mathbf{I}_{sk}$. By the adopted transposition approach, the vectors of the strand currents flowing into different line sections are related as follows. Assuming for the first section $\mathbf{I}_{s1} = [I_1\ I_2\ I_3\ \ldots\ I_n]^T = \mathbf{I}$, the current into Section II is given by $\mathbf{I}_{s2} = [I_n\ I_1\ I_2\ \ldots\ I_{n-1}]^T = \mathbf{T}^{-1}\,\mathbf{I}$, the current into Section III is $\mathbf{I}_{s3} = [I_{n-1}\ I_n\ I_1\ \ldots\ I_{n-2}]^T = (\mathbf{T}^{-1})^2\,\mathbf{I}$, etc., when the $n\times n$ permutation matrix $\mathbf{T}$ is given by

$$\mathbf{T} = \begin{bmatrix} \begin{pmatrix} 0 \\ 0 \\ \vdots \\ 0 \\ 1 \end{pmatrix} & \begin{pmatrix} 1 & 0 & \cdots & 0 \\ 0 & 1 & \cdots & 0 \\ \vdots & \vdots & \ddots & \vdots \\ 0 & 0 & \cdots & 1 \\ 0 & 0 & \cdots & 0 \end{pmatrix} \end{bmatrix}. \tag{14}$$

Therefore, the current vector for the generic kth section can be obtained by

$$\mathbf{I}_{sk} = \left(\mathbf{T}^{-1}\right)^{k-1}\mathbf{I}. \tag{15}$$

Different types of permutation can be easily obtained by suitably modifying the matrix $\mathbf{T}$. In the following, the transposition matrix $\mathbf{T}$ in (14) is used as it is easy to understand and implement. All the strands complete the permutation, i.e., assume identical positions, when the number of line sections m coincides with the number n of strands, i.e., $m = n$, or more generally, when $m = kn$ being k an integer number.

According to the notation adopted, the voltage drop vector $\mathbf{V}_{sk}$ along the generic kth section is given by

$$\mathbf{V}_{sk} = \begin{bmatrix} V_{1,sk} \\ V_{2,sk} \\ \vdots \\ V_{n,sk} \end{bmatrix} = \mathbf{Z}_s\mathbf{I}_{sk}. \tag{16}$$

The coefficient $V_{i,sk}$ of the voltage vector $\mathbf{V}_{sk}$ is the voltage drop on the conductor occupying the ith position in the kth section, and not the voltage drop on the ith conductor that, in the considered section, has been moved in a different position due to the transposition (see again Fig. 3). The vector $\mathbf{V}_{pk}$ containing the voltage drops along each strand can be obtained from $\mathbf{V}_{sk}$ by reordering its coefficients. It yields: $\mathbf{V}_{p1} = [V_{1,s1}\ V_{2,s1}\ V_{3,s1}\ \ldots\ V_{n,s1}]^T$; $\mathbf{V}_{p2} = [V_{2,s2}\ V_{3,s2}\ \ldots\ V_{n,s2}\ V_{1,s2}]^T = \mathbf{T}\,\mathbf{V}_{s2}$; $\mathbf{V}_{p3} = [V_{3,s2}\ V_{4,s3}\ \ldots\ V_{n,s3}\ V_{1,s3}\ V_{2,,s3}]^T = \mathbf{T}^2\,\mathbf{V}_{s3}$; etc. Therefore, the voltage drop vector $\mathbf{V}_{pk}$ can be obtained for the generic kth section by

$$\mathbf{V}_{pk} = \mathbf{T}^{k-1}\mathbf{V}_{sk}. \tag{17}$$

The voltage drop vector $\mathbf{V} = [V_1\ V_2\ V_3\ \ldots\ V_n]^T$ along the n wires for the total length ℓ of the litz wire can be easily obtained by summing the voltage drops $\mathbf{V}_{pk}$ along all different line sections as

$$\mathbf{V} = \sum_{k=1}^{m}\mathbf{V}_{pk} \tag{18}$$

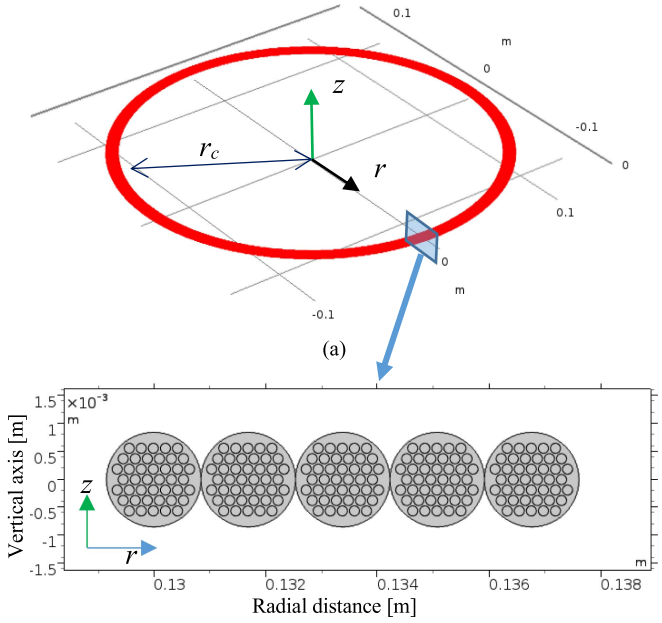

Fig. 4. (a) Circular planar coil. (b) Cross section of the planar coil with $N = 5$.

and, via (16) and (17), it yields

$$\mathbf{V} = \sum_{k=1}^{m} \mathbf{T}^{k-1} \mathbf{Z}_s \mathbf{I}_{sk}. \tag{19}$$

Finally, the voltage vector $\mathbf{V}$ can be expressed as function of $\mathbf{I}$ via (15) as

$$\mathbf{V} = \sum_{k=1}^{m} \mathbf{T}^{k-1} \mathbf{Z}_s \left(\mathbf{T}^{-1}\right)^{k-1} \mathbf{I}. \tag{20}$$

The impedance matrix $\hat{\mathbf{Z}}$ of a litz wire applying the proposed transposition with m permutations is then given by

$$\hat{\mathbf{Z}} = \sum_{k=1}^{m} \mathbf{T}^{k-1} \mathbf{Z}_s \left(\mathbf{T}^{-1}\right)^{k-1}. \tag{21}$$

The litz wire current I_W can also be expressed via (7) and (8), when considering the modified admittance $\hat{\mathbf{Y}} = \hat{\mathbf{Z}}^{-1}$, as

$$I_W = \begin{bmatrix} 1 & 1 & \cdots & 1 \end{bmatrix} \hat{\mathbf{Y}} \begin{bmatrix} 1 \\ 1 \\ \vdots \\ 1 \end{bmatrix} V_a = V_a \sum_{i=1}^{n} \sum_{j=1}^{n} \hat{Y}_{ij} \tag{22}$$

being $\hat{Y}_{ij}$ the ijth coefficient of matrix $\hat{\mathbf{Y}}$.

From (9), the impedance of the litz wire cable is then given by

$$\hat{Z}_W = \frac{V_a}{I_W} = \frac{1}{\sum_{i=1}^{n} \sum_{j=1}^{n} \hat{Y}_{ij}}. \tag{23}$$

The number of transpositions m can be selected as compromise between the ideal transposition, which can be obtained for a number of sections that tends to infinite $(m \to \infty)$ and parallel strand configuration $(m = 1)$. A recommended choice is to select $m = n$, as minimum number of sections, to ensure the full transposition of all strands. It should be noted that mathematical criterion adopted for the transposition (i.e., ideal pattern) cannot fit exactly the physical configuration. However, when n is quite large and m is large enough, it is realistic to assume that the adopted transposition is quite close to ideal.

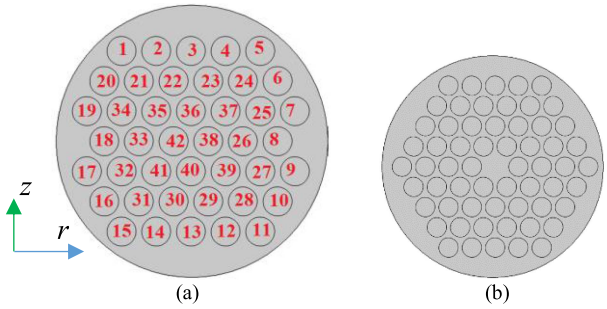

Fig. 5. (a) Position numbering of the strands in the cross section of litz wire#1 with $n = 42$ strands. (b) Cross section of litz wire#2 with $n = 60$ strands.

Finally, the formula in (23) must consider the difference in length between a twisted strand and a straight litz wire [39]. Assuming for simplicity a helical shape for a strand path, the factor k_p of the shortening of length due to the bunching process is given by

$$k_p = \frac{\sqrt{p^2 + c^2}}{p} \tag{24}$$

being c the circumference of the litz cable. Thus, (23) must be modified introducing the factor k_p as

$$\hat{Z}_W = k_p \frac{1}{\sum_{k=1}^{n} \sum_{i=1}^{n} \hat{Y}_{kj}}. \tag{25}$$

D. Numerical Simulation

The $n \times n$ impedance matrix of a parallel strand line is obtained by postprocessing of the 2-D-FEA in the frequency domain. For the numerical simulation, the eddy currents equation is adopted

$$\nabla \times \left(\frac{1}{\mu} \nabla \times \mathbf{A}\right) + j\omega\sigma\mathbf{A} = \mathbf{J_s} \tag{26}$$

being $\mathbf{A}$ the magnetic vector potential, μ the magnetic permeability, σ the conductivity, and $\mathbf{J_s}$ the current density source.

The simulations of the coils are performed assuming a 2-D axial symmetric configuration to model a circular coil. The calculations are performed in COMSOL modeling each strand as a separate coil function and extracting the current, as described in Section II-B.

It should be noted that the impedance matrix is calculated by a 2-D axial symmetric FEA, approximating the multiturn structure of a planar circular coil by means of series-connected multistrand coil, as schematically shown in Fig. 4.

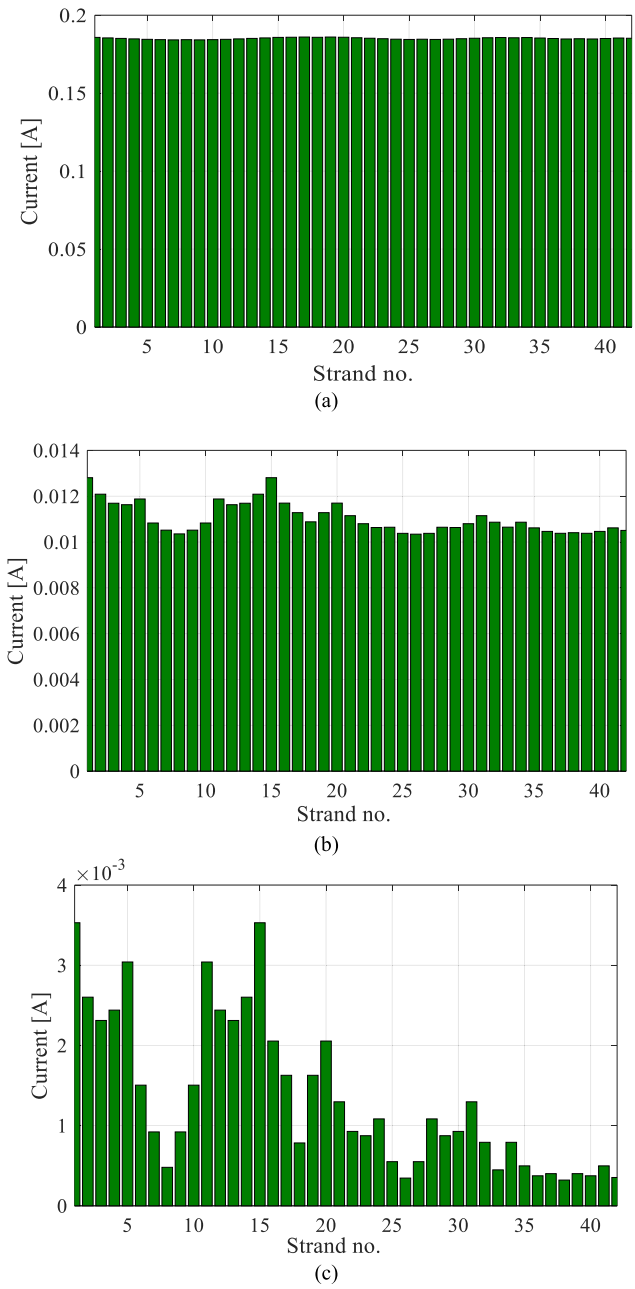

Fig. 6. Current distributions in the $n = 42$ parallel strands obtained by a 2-D FEA for case #1: (a) 1 kHz, (b) 20 kHz, and (c) 200 kHz.

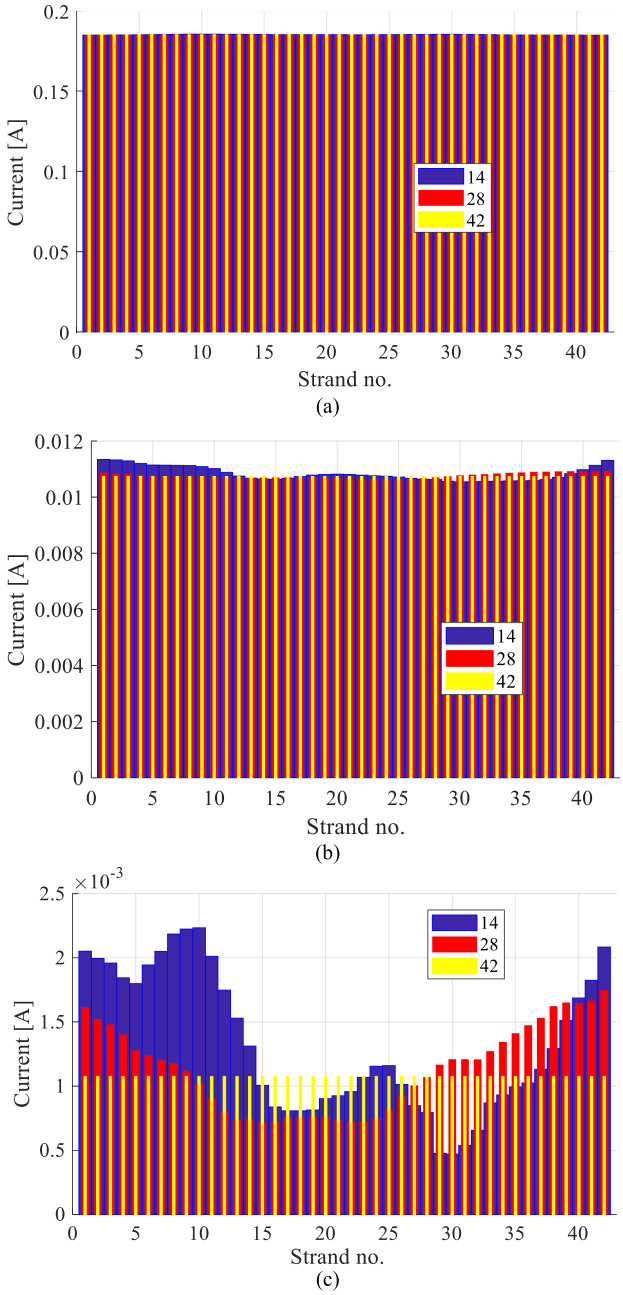

Fig. 7. Current distributions in the 42 strands of the litz wire, varying the number of total transpositions ($m = 14$, $m = 28$, and $m = 42$): (a) 1 kHz, (b) 20 kHz, and (c) 200 kHz.

III. Applications

To validate the proposed method, two single bundle litz wires are considered. The wire#1 is composed by $n = 42$ strands with strand diameter $d = 0.18$ mm, cable diameter $d_c = 1.7$ mm, pitch $p = 28$ mm, and $k_p = 1.02$, whereas the wire#2 is composed by $n = 60$ strands with strand diameter $d = 0.1$ mm, cable diameter $d_c = 1$ mm, pitch $p = 12$ mm, and $k_p = 1.03$. The cross sections of litz wires #1 and #2 are shown in Fig. 5.

Three different geometrical configurations are tested as listed in the following.

Case #1) planar circular coil, inner radius $r_c = 13$ cm and number of turns $N = 5$, wire#1.

Case #2) stacked helicoidal coil, inner radius $r_c = 8$ cm, number of turns $N = 20$, wire#1.

Case #3) planar circular coil, inner radius $r_c = 13.25$ cm, number of turns $N = 5$, wire#2.

In all previous test cases, the value of k_p was calculated by (24) to take into account the shortening of the strand length due to bunching process. The current distribution in $n = 42$ strands of wire#1 obtained from (7) postprocessing the 2-D FEA solution of a uniform MTL with parallel strands, i.e., no bunching or twisting, is shown in Fig. 6 for test case #1 considering three different frequencies: (a) $f = 1$ kHz, (b) $f = 20$ kHz, and (c) $f = 200$ kHz. It can be observed that the currents are different

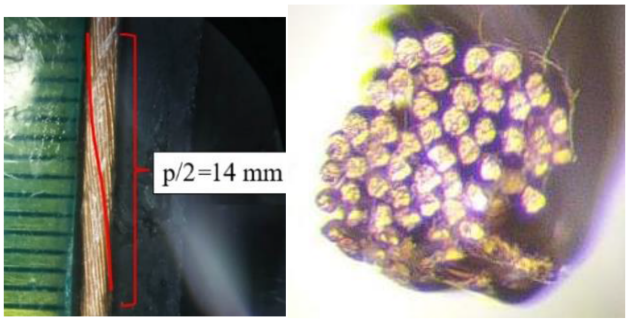

Fig. 8. Microscope images of the adopted litz wire: (a) longitudinal view; (b) cut section.

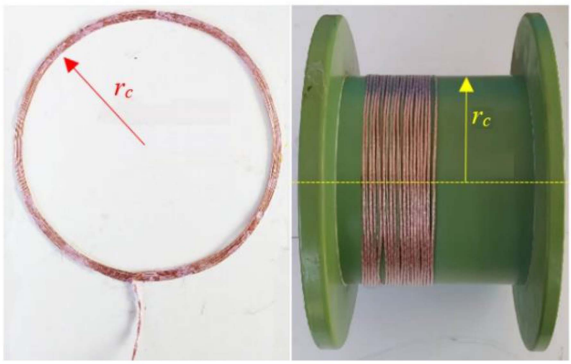

Fig. 9. Coils used in the experiments: (a) test case #1—planar circular coil with $N = 5$ turns; (b) test case #2—helicoidal coil with $N = 20$ turns.

in each strand depending on its relative position in the wire section and the differences increase with increasing frequency.

Then, the proposed transposition algorithm is applied assuming different numbers m of discrete transpositions. The obtained current distribution in $n = 42$ strands is shown in Fig. 7 for a different number of transpositions ($m = 14$, $m = 28$, and $m = 42$) at three different frequencies ($f = 1$ kHz, $f = 20$ kHz, and $f = 200$ kHz). The obtained results demonstrate that the current in all strands tends to be identical as m increases. It means that the current distribution tends to a similar value in all strands, thus demonstrating that each strand has roughly the same path and impedance, which was the initial goal of the proposed transposition procedure.

A comparison was made with the experimental results to validate the proposed simulation method based on discrete transposition. The microscope images of the longitudinal and cut section view of the adopted litz wire#1 are shown in Fig. 8, whereas the test coils used in the experiments are shown in Fig. 9. The ac resistance $R_{\rm ac}$ and the ac-to-dc resistance ratio F_R for the considered test cases #1–3 have been measured adopting a precision *LCR* meter, model Keysight E4980A in the frequency range from 0 to 1 MHz. The experimental test set-up is shown in Fig. 10. The simulations carried out by the proposed procedure are referenced in the following figures as "2-D FEA + transposition," whereas those considering a

Fig. 10. Experimental set-up for test case #1.

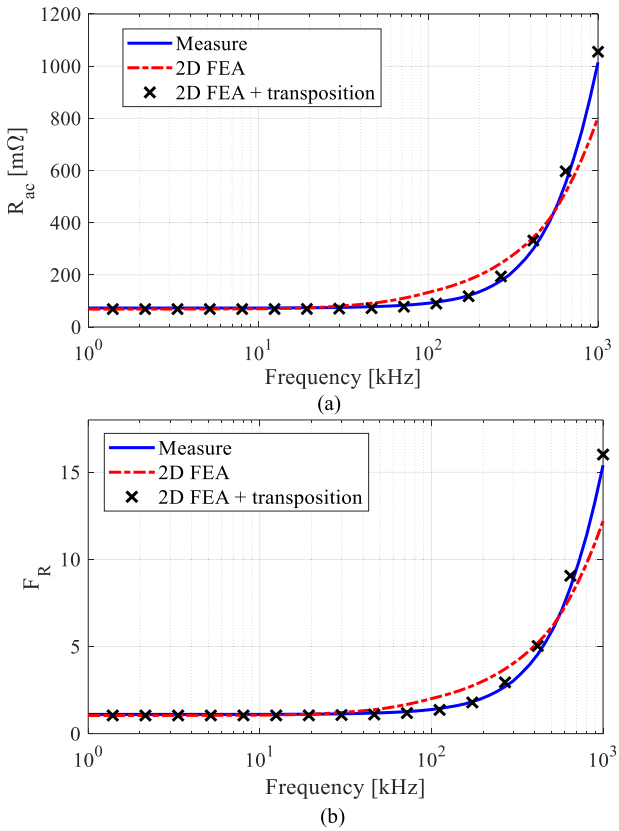

Fig. 11. Test case #1 (planar circular coil, inner radius $r_c = 13$ cm, number of turns $N = 5$; wire#1: number of strands $n = 42$, strand diameter $d = 0.18$ mm): (a) ac resistance $R_{\rm ac}$; (b) ac-to-dc resistance ratio F_R.

uniform litz wire (i.e., parallel strands without transposition) are referenced as "2-D FEA." The measured values for the three test cases are compared with simulations results obtained by the proposed procedure adopting $m = n$, as shown in Figs. 11 –13, respectively.

As can be seen, the results provided by the proposed method are in excellent agreement with the measurements for different geometric configurations and types of litz wires. On the contrary, the simple 2-D FEA provides inaccurate results and is therefore

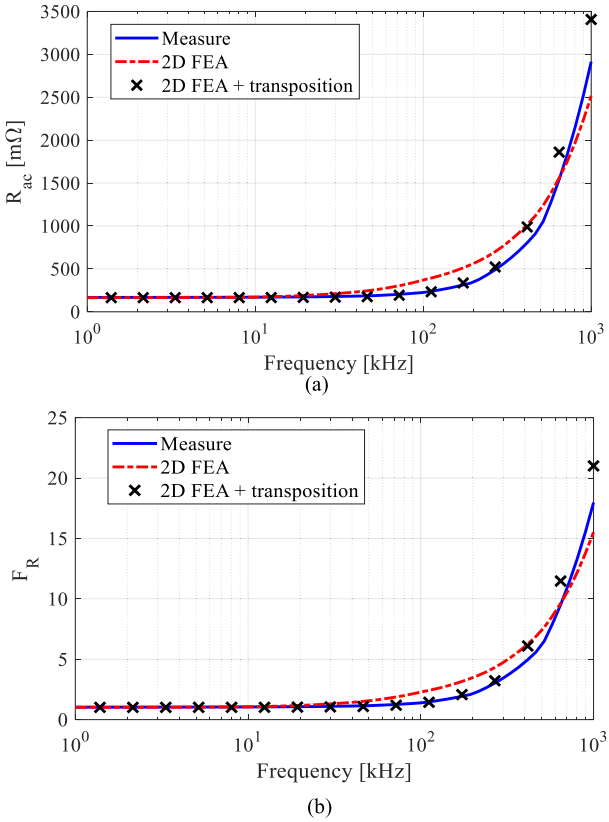

Fig. 12. Test case #2 (staked helicoidal coil, inner radius $r_c = 13$ cm, number of turns $N = 20$; wire#1: number of strands $n = 42$, strand diameter $d = 0.18$ mm): (a) ac resistance $R_{\rm ac}$; (b) ac-to-dc resistance ratio F_R.

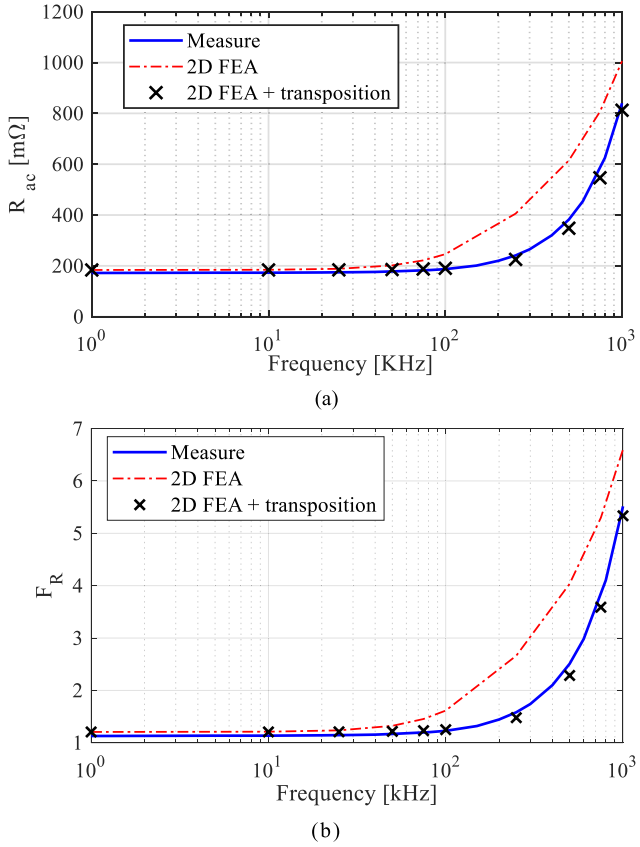

Fig. 13. Test case #3 (planar circular coil, inner radius $r_c = 13.25$ cm, number of turns $N = 5$; wire#2: number of strands $n = 60$, strand diameter $d = 0.1$ mm): (a) ac resistance $R_{\rm ac}$; (b) ac-to-dc resistance ratio F_R.

not able to model the litz wire behavior, as expected, demonstrating the importance of the strand transposition algorithm. Finally, at higher frequencies, a certain error appears as we adopted the eddy current equations formulation, which are valid only at low frequency.

As the previous numerical results are dependent on the number of permutations *m,* a sensitive analysis has been performed for the test cases #1 and #2 calculating the average relative error $e_\Sigma(m)$ of the ac-to-dc resistance ratio F_R in all frequency spectrum under examination by the following formula:

$$e_\Sigma(m) = \frac{1}{M}\sum_{k=1}^{M}\frac{|F_{R,\text{meas}}(\omega_k) - F_{R,\text{num}}(\omega_k, m)|}{|F_{R,\text{meas}}(\omega_k)|} \quad (27)$$

where $F_{R,\text{meas}}$ and $F_{R,\text{num}}$ represent the values obtained by measurements and numerical simulations, respectively. It should be noted that (27) evaluates the error $e_\Sigma(m)$ in a given frequency band, i.e., $\omega_k = 2\pi f_k$, with M samples such that 1 kHz $\leq f_k \leq$ 200 kHz for k from 1 to M. The results obtained by varying the number m of discrete transpositions up to $3n$ and assuming $M = 16$ in (27) are shown in Fig. 14 and show how the accuracy increases considerably up to $m = n$, whereas a further increase in the number m of transpositions does not significantly improve accuracy. The error $e_\Sigma(m)$ in the considered test cases #1 and 2 is quite small, $e_\Sigma(m) < 0.05$ for $m \geq n$, and converges for $m \geq n$. From the error analysis, we can state that $n = m$ is a reasonable discretization step of the litz wire to obtain a satisfactory accuracy by means of the proposed transposition approach, at least for the considered litz wire. Thus introducing the error $e(\omega)$ as function of the angular frequency $\omega = 2\pi f$ defined as

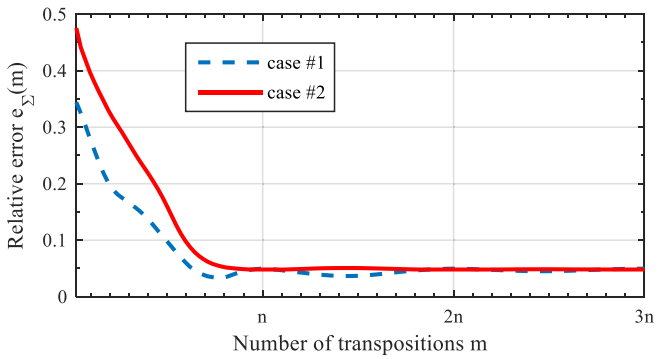

Fig. 14. Average relative error $e_\Sigma(m)$ versus number m of transpositions for test cases #1 and #2 in the frequency band $f =$ 1 kHz – 200 kHz.

$$e(\omega) = \frac{|F_{R,\text{meas}}(\omega) - F_{R,\text{num}}(\omega, m)|}{|F_{R,\text{meas}}(\omega)|} \quad (28)$$

it is possible to evaluate $e(\omega)$ for the test cases #1 and 2 assuming $n = m$, as shown in Fig. 15.

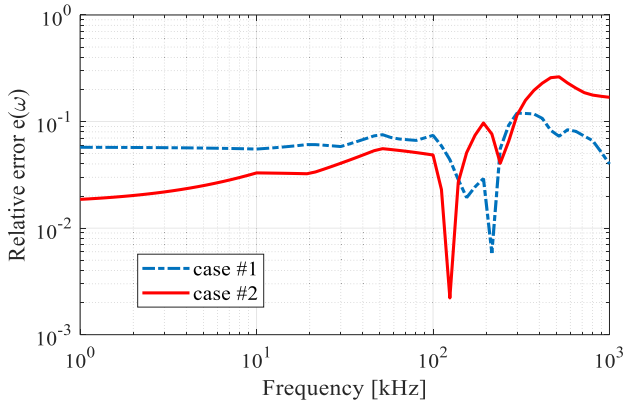

Fig. 15. Relative error $e(\omega)$ versus angular frequency ω for test cases #1 and #2 in the frequency range $f = 1$ kHz – 1 MHz assuming $n = m$.

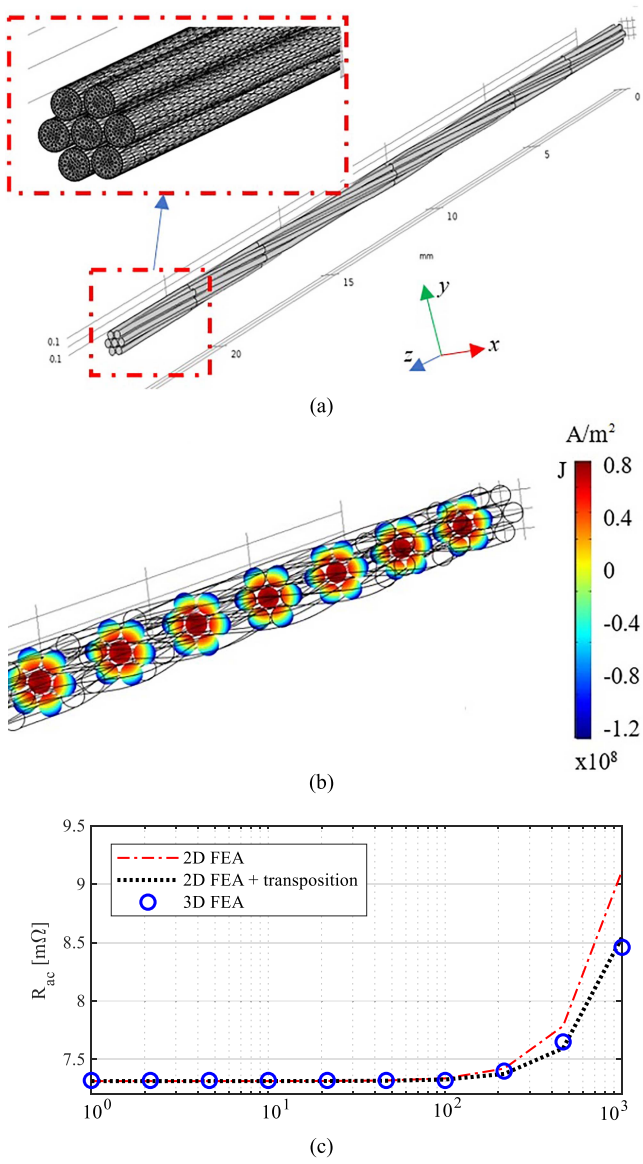

Fig. 16. (a) Litz wire configuration with 3-D FEA discretization. (b) Map of the current density distribution at 1 MHz. (c) Calculated ac resistance $R_{\rm ac}$.

Finally, a simple test was performed to compare the results obtained with the proposed method (2-D FEA + transposition) with those obtained from a complete 3-D FEA for a litz wire with simple configuration. The considered cable is composed by $n = 7$ strands with diameter $d = 0.1$ mm and pitch $p = 24$ mm. The cable has been discretized using 1 254 128 tetrahedral elements. The configuration mesh and the obtained results are shown in Fig. 16 demonstrating an excellent agreement. In the considered case, the computational cost of the 3-D FEA is much higher, with a solution time of 6 h and 34 min using an two Intel Xeon X5260 processors against a time of 5 s for the 2-D FEA simulation and few milliseconds for the transposition process.

IV. Conclusion

A new approach has been proposed for modeling a single bundle litz wire by simulation. The ac resistance is obtained by applying Ohm's law to a multistrand structure given by a series cascade of uniform MTL sections with parallel strands whose impedance matrix is extracted from a 2-D FEA. A mathematical algorithm of discrete transposition is applied to the cascade of identical uniform MTL sections to simulate the ideal pattern of a litz wire where all strands have the same path due to the bunching and twisting process.

The proposed method compared with measurements and 3-D numerical results proved to be very accurate and efficient. The computational cost is not expensive and comparable with a traditional 2-D FEA, which is much lower than a complex 3-D simulation, whereas the simple 2-D FEA without strand transposition algorithm proposed in this work is not accurate.

References

[1] G. A. Covic and J. T. Boys, "Inductive power transfer," *Proc. IEEE*, vol. 101, no. 6, pp. 1276–1289, Jun. 2013.
[2] C. T. Rim and C. Mi, *Wireless Power Transfer for Electric Vehicles and Mobile Devices*. Hoboken, NJ, USA: Wiley, 2017.
[3] P. L. Dowell, "Effects of eddy currents in transformer windings," *Proc. IET*, vol. 113, no. 8, pp. 1387–1394, Aug. 1966.
[4] J. A. Ferreira, "Analytical computation of AC resistance of round and rectangular litz wire windings," *IET Proc. B Electric Power Appl.*, vol. 139, no. 1, pp. 21–25, Jan. 1992.
[5] J. A. Ferreira, "Improved analytical modeling of conductive losses in magnetic components," *IEEE Trans. Power Electron.*, vol. 9, no. 1, pp. 127–131, Jan. 1994.
[6] C. R. Sullivan, "Optimal choice for number of strands in a litz-wire transformer winding," *IEEE Trans. Power Electron.*, vol. 14, no. 2, pp. 283–291, Mar. 1999.
[7] C. R. Sullivan, "Computationally efficient winding loss calculation with multiple windings, arbitrary waveforms, and two- or three-dimensional field geometry," *IEEE Trans. Power Electron.*, vol. 16, no. 1, pp. 142–150, Jan. 2001.
[8] J. Acero, R. Alonso, J. M. Burdio, L. A. Barragan, and D. Puyal, "Frequency-dependent resistance in litz-wire planar windings for domestic induction heating appliances," *IEEE Trans. Power Electron.*, vol. 21, no. 4, pp. 856–866, Jul. 2006.
[9] H. Rossmanith, M. Doebroenti, M. Albach, and D. Exner, "Measurement and characterization of high frequency losses in nonideal litz wires," *IEEE Trans. Power Electron.*, vol. 26, no. 11, pp. 3386–3394, Nov. 2011.
[10] Q. Deng et al., "Frequency-dependent resistance of litz-wire square solenoid coils and quality factor optimization for wireless power transfer," *IEEE Trans. Ind. Electron.*, vol. 63, no. 5, pp. 2825–2837, May 2016.
[11] I. Lope, J. Acero, and C. Carretero, "Analysis and optimization of the efficiency of induction heating applications with litz-wire planar and solenoidal coils," *IEEE Trans. Power Electron.*, vol. 37, no. 7, pp. 5089–5101, Jul. 2016.

[12] D. Barth, B. Klaus, and T. Leibfried, "Litz wire design for wireless power transfer in electric vehicles," in *Proc. IEEE Wireless Power Transfer Conf.*, 2017, pp. 1–4.
[13] K. Umetani, S. Kawahara, J. Acero, H. Sarnago, Ó. Lucía, and E. Hiraki, "Analytical formulation of copper loss of litz wire with multiple levels of twisting using measurable parameters," *IEEE Trans. Ind. Appl.*, vol. 57, no. 3, pp. 2407–2420, May/Jun. 2021.
[14] J. Acero, I. Lope, J. M. Burdio, C. Carretero, and R. Alonso, "Loss analysis of multistranded twisted wires by using 3D-FEA simulation," in *Proc. IEEE Workshop Control Model. Power Electron.*, 2014, pp. 1–6.
[15] A. Rosskopf, E. Bar, and C. Joffe, "Influence of inner skin- and proximity effects on conduction in litz wires," *IEEE Trans. Power Electron.*, vol. 29, no. 10, pp. 5454–5461, Oct. 2014.
[16] A. Rosskopf, E. Bar, C. Joffe, and C. Bonse, "Calculation of power losses in litz wire systems by coupling FEM and PEEC method," *IEEE Trans. Power Electron.*, vol. 31, no. 9, pp. 6442–6449, Sep. 2016.
[17] A. Rosskopf, "Calculation of frequency dependent power losses in inductive systems with litz wire conductors by a coupled numerical approach," Ph.D. dissertation, Dept. Inf. Technol. Elect. Elect. Eng., Friedrich-Alexander-Universität, Erlangen, Germany, 2018.
[18] E. Plumed, J. Acero, I. Lope, and C. Carretero, "3D finite element simulation of litz wires with multilevel bundle structure," in *Proc. IEEE 44th Annu. Conf. Ind. Electron. Soc.*, 2018, pp. 3479–3484, doi: 10.1109/IECON.2018.8591341.
[19] S. Ehrlich, H. Rossmanith, M. Sauer, C. Joffe, and M. März, "Fast numerical power loss calculation for high-frequency litz wires," *IEEE Trans. Power Electron.*, vol. 36, no. 2, pp. 2018–2032, Feb. 2021.
[20] C. Carretero, J. Acero, and R. Alonso, "TM-TE decomposition of power losses in multi-stranded litz-wires used in electronic devices," *Prog. Electromagn. Res.,* vol. 123, pp. 83–103, Dec. 2012.
[21] J. Lyu, H. C. Chen, Y. Zhang, Y. Du, and Q. S. Cheng, "Litz wire and uninsulated twisted wire assessment using a multilevel PEEC method," *IEEE Trans. Power Electron.*, vol. 37, no. 2, pp. 2372–2381, Feb. 2022.
[22] N. J. Salk and C. M. Cooke, "A versatile simulation-assisted layered mesh analysis for generalized litz wire performance," *IEEE Trans. Magn.,* vol. 58, no. 6, Jun. 2022, Art. no. 8600208.
[23] D. Lin, C. Lu, N. Chen, and P. Zhou, "An efficient method for litz-wire AC loss computation in transient finite element analysis," *IEEE Trans. Magn.*, vol. 58, no. 5, May 2022, Art. no. 7400710.
[24] N. J. Salk and C. M. Cooke, "Calculation of AC losses in multi-phase litz coil systems," in *Proc. IEEE Transp. Electrific. Conf. Expo.*, 2022, pp. 594–599, doi: 10.1109/ITEC53557.2022.9813754.
[25] A. Rosskopf and C. Brunner, "Enhancing litz wire power loss calculations by combining a sparse strand element equivalent circuit method with a Voronoi-based geometry model," *IEEE Trans. Power Electron.*, vol. 37, no. 9, pp. 11450–11456, Sep. 2022.
[26] J. Lyu, H. Chen, Y. Zhang, Y. Du, and Q. S. Cheng, "Fast simulation of litz wire using multilevel PEEC method," *IEEE Trans. Power Electron.*, vol. 35, no. 12, pp. 12612–12616, Dec. 2020.
[27] J. Panchal, A. Lehikoinen, and P. Rasilo, "Efficient finite element modelling of litz wires in toroidal inductors," *IET Power Electron.*, vol. 14, pp. 2610–2619, 2021.
[28] X. Xiangwang and C. Wei, "Solution of litz wire winding loss based on segmented equivalent circuit method," *Eng. Technol. II—Elect. Eng.*, no. 3, pp. 30–35, 2017.
[29] X. Nan and C. R. Sullivan, "An equivalent complex permeability model for litz-wire windings," in *Proc. 40th IAS Annu. Meeting Conf. Rec. Ind. Appl. Conf.*, 2005, vol. 3, pp. 2229–2235, doi: 10.1109/IAS.2005.1518758.
[30] M. Etemadrezaei and S. M. Lukic, "Equivalent complex permeability and conductivity of litz wire in wireless power transfer systems," in *Proc. IEEE Energy Convers. Congr. Expo.*, 2012, pp. 3833–3840.
[31] Y. Otomo, H. Igarashi, H. Sano, and T. Yamada, "Analysis of litz wire losses using homogenization-based FEM," *IEEE Trans. Magn.*, vol. 57, no. 8, Aug. 2021, Art. no. 7402409.
[32] C. R. Paul and J. W. McKnight, "Prediction of crosstalk involving twisted pairs of wires—Part I: A transmission-line model for twisted-wire pairs," *IEEE Trans. Electromagn. Compat.*, vol. EMC-21, no. 2, pp. 92–105, May 1979.
[33] C. R. Paul and J. W. McKnight, "Prediction of crosstalk involving twisted pairs of wires—Part II: A simplified low-frequency prediction model," *IEEE Trans. Electromagn. Compat.*, vol. EMC-21, no. 2, pp. 105–114, May 1979.
[34] C. Buccella, M. Feliziani, G. Manzi, and F. Maradei, "Prediction of voltage and current propagation in twisted wire pairs (TWPs) by a circuit model," in *Proc. Int. Symp. Electromagn. Compat.*, 2005, pp. 51–55, doi: 10.1109/ISEMC.2005.1513470.
[35] S. Cristina and M. Feliziani, "A finite element technique for multiconductor cable parameters calculation," *IEEE Trans. Magn.*, vol. 25, no. 4, pp. 2986–2988, Jul. 1989.
[36] M. Feliziani and F. Maradei, "Edge element analysis of complex configurations in presence of shields," *IEEE Trans. Magn.*, vol. 33, no. 2, pp. 1548–1551, Mar. 1997.
[37] M. Feliziani and F. Maradei, "Fast computation of quasi-static magnetic fields around nonperfectly conductive shields," *IEEE Trans. Magn.*, vol. 34, no. 5, pp. 2795–2798, Sep. 1998.
[38] M. Feliziani, "Subcell FDTD modeling of field penetration through lossy shields," *IEEE Trans. Electromagn. Compat.*, vol. 54, no. 2, pp. 299–307, Apr. 2012.
[39] Elektrisola. "Litz wire, HF-litz, high frequency litz wire, litz wire for high efficiency," Accessed: May 23, 2022. [Online]. Available: https://www.elektrisola.com/en/Litz-Wire/Info
[40] C. R. Sullivan, "Cost-constrained selection of strand diameter and number in a litz-wire transformer winding," *IEEE Trans. Power Electron.,* vol. 16, no. 2, pp. 281–288, Mar. 2001.
[41] T. Campi, S. Cruciani, V. De Santis, F. Maradei, and M. Feliziani, "Numerical characterization of the magnetic field in electric vehicles equipped with a WPT system," *Wireless Power Transfer*, vol. 4, no. 2, pp. 78–87, 2017.